Supporting Information

Construction of phase-separated Co/MnO synergistic catalysts and integration onto sponge for rapid removing multiple contaminants

Mengting Liu[a], Wanyu Zhang[a], Ruiting Ni[a], Zhenxiao Wang[a], Hongyao Zhao[a], Xiu Zhong[a], Yanyun Wang[a], Danhong Shang[a], Zengjing Guo[b], Edison Huixiang Ang[b,*], Fu Yang[a,*]

[a] School of Environmental and Chemical Engineering, Jiangsu University of Science and Technology, Zhenjiang 212003, Jiangsu, P. R. China
[b] Natural Sciences and Science Education, National Institute of Education, Nanyang Technological University, Singapore 637616, Singapore
[c] School of Chemistry and Chemical Engineering, Liaocheng University, Liaocheng 252000, Shandong, PR China

*Corresponding Authors: E-mail addresses: edison.ang@nie.edu.sg (E. H. Ang), fuyang@just.edu.cn (F. Yang)

Table. S1 ICP measurement results of Mn and Co content in different comparative catalysts and metal leaching fraction of different catalysts.

Table. S2 Detailed structural properties including surface area, total pore volume, and average pore diameter of MnOOH, Mn_2O_3-600, Mn_3O_4/C-600, Mn_3O_4/Co-600, MnO@Co/C-500, MnO@Co/C-600, MnO@Co/C-600.

Table. S3 Toxicity assessment of various intermediates from tetracycline bisphenol A degradation.

Fig. S1 Structural formula of BPA.

Fig. S2. Representive SEM of (a)MnOOH, (b) Mn_2O_3-600, (c)Mn_3O_4/Co-600.

Fig. S3 (a,b) N_2 adsorption/desorption isotherm and (c,d) corresponding pore size distribution of comparative catalysts MnOOH, Mn_2O_3-600, Mn_3O_4/C-600, Mn_2O_3/Co-600, MnO@Co/C-500, MnO@Co/C-600, MnO@Co/C-700.

Fig. S4 Jahn-Teller distortions for octahedral Mn complex.

Fig. S5 Electrochemical impedance spectra (EIS) for different samples

Fig. S6 Charging current density difference and cyclic voltammetry (CV) scanning rate of catalysts (a), analysis of the electrochemical active surface area (ECSA): Cyclic voltammetric curves for different scan rates (20-120 mV s^{-1}) and (b) Mn_3O_4/C-600, (c) MnO@Co/C-500, (d) MnO@Co/C-600, (e) MnO@Co/C-700 samples in the range from -0.2 to 0.3 V vs. RHE.

Fig. S7 (a) Time-dependent BPA degradation course curves over MnO@Co/C-600 using different PMS dosages, and (b) corresponding kinetic curves: $\ln(C_0/C)$ v.s. reaction time; (c) Time-dependent BPA degradation course curves over MnO@Co/C-600 using catalyst dosages, and (d) corresponding kinetic curves: $\ln(C_0/C)$ v.s. reaction time; (e) Time-dependent BPA degradation course curves over MnO@Co/C-600 using different BPA concentration, and (f) corresponding kinetic curve: $\ln(C_0/C)$ v.s. (g) Time-dependent BPA degradation course curves over MnO@Co/C-600 using different BPA concentration, and (h) corresponding kinetic curve: $\ln(C_0/C)$ v.s. reaction time.

Fig. S8 Contribution of different quenchers to quenched active radicals.

Fig. S9 Time-dependent BPA degradation course curves over MnO@Co/C-600 using different anion.

Fig. S10 BPA degradation course curves by MnO@Co/C-600 system in actual water samples; (b) Different pollutations degradation course curves in MnO@Co/C-600 system; (c) The cycling experiment results of MnO@Co/C-600 in activation of PMS for BPA degradation.

Fig. S11 (a) Degradation progress curves of BPA using the MnO@Co/C-600 system in authentic water samples; (b) Degradation progress curves of different pollutants in the MnO@Co/C-600 system; (c) Results of cycling experiments with MnO@Co/C-600 in activating PMS for BPA degradation; (d) Total Organic Carbon (TOC) removal progress curves using the MnO@Co/C-600 system for different pollutants;.

Fig. S12 (a) The schematic diagram of circulation filter integrated device; (b) BPA degradation course curves by MnO@Co/C-600 system under flow-through conditions;

Fig. S13 Time-dependent surface temperature thermal IR images of wet MnO@Co/C-600 samples under one sun irradiation in air.
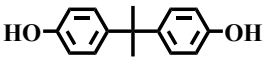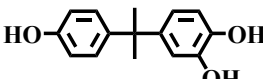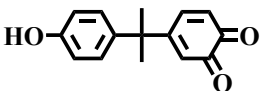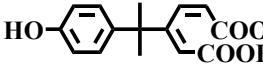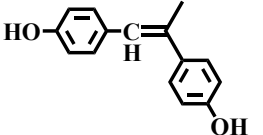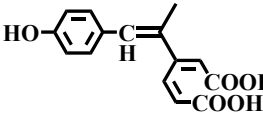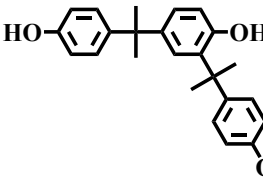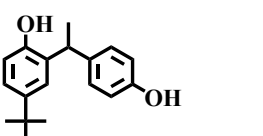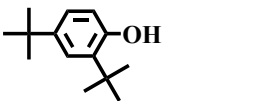
Table. S1 ICP measurement results of Mn and Co content in different comparative catalysts and metal leaching fraction of different catalysts.

Samples	Mn (wt. %)	Co (wt. %)	Total (wt. %)	Co leaching (wt. %)	Mn leaching (wt. %)
MnOOH	58.90	/	58.90	/	/
Mn_2O_3-600	64.01	/	64.01	/	/
Mn_3O_4/C-600	43.86	/	43.86	/	/
Mn_3O_4/Co-600	45.85	6.05	51.90	20.3	12.4
MnO@Co/C-500	44.88	6.27	51.15	/	/
MnO@Co/C-600	49.24	6.89	56.13	3.9	2.1
MnO@Co/C-700	51.86	8.47	60.33	/	/

Table. S2 Detailed structural properties including surface area, total pore volume, and average pore diameter of MnOOH, Mn_2O_3-600, Mn_3O_4/C-600, Mn_3O_4/Co-600, MnO@Co/C-500, MnO@Co/C-600, and MnO@Co/C-600.

Samples	S_{BET} (m^2/g)	Total pore volume (cm^3/g)	Average pore diameter (nm)
MnOOH	70.8	0.23	13.0
Mn_2O_3-600	7.9	0.06	31.8
Mn_3O_4/C-600	155.2	0.14	3.5
Mn_3O_4/Co-600	21.2	0.06	10.4
MnO@Co/C-500	28.9	0.30	41.6
MnO@Co/C-600	112.7	0.35	12.4
MnO@Co/C-700	2.5	0.02	29.7

Samples	S_{BET} (m^2/g)	Total pore volume (cm^3/g)	Average pore diameter (nm)

Table. S3 Toxicity assessment of various intermediates from tetracycline bisphenol A degradation.

Compounds	Molecular Formula	Acute toxicity			
		Fish LC50 (96h mg/L)	Daphnia magna LC50 (48h mg/L)	Pyriformis IGC50 (48h mg/L)	Oral rat LD50 (mg/kg)
P	HO—⬡—⬡—OH	3.24	1.58	5.30	4108.99
P1	HO—⬡—⬡(OH)—OH	2.32	1.59	4.55	1140.28
P2	HO—⬡—⬡=O (=O)	2.21	9.73	0.98	2346.85
P3	HO—⬡—⬡(COOH)(COOH)	-	-	-	-
P4	HO—⬡—C=CH—⬡—OH	0.46	2.02	5.92	3683.42
P5	HO—⬡—C=CH—⬡(COOH)(COOH)	-	-	-	-
P6	HO—⬡—⬡(—OH)—⬡—OH	0.21	0.40	0.11	558.97
P7	OH—⬡—CH—⬡—OH	0.37	0.80	1.70	2554.43
P8	⬡(—OH)	2.04	0.56	6.40	1229.06

Not harmful >100 mg/L	Harmful 10-100 mg/L	Toxic 1-10 mg/L	Very toxic <1 mg/L
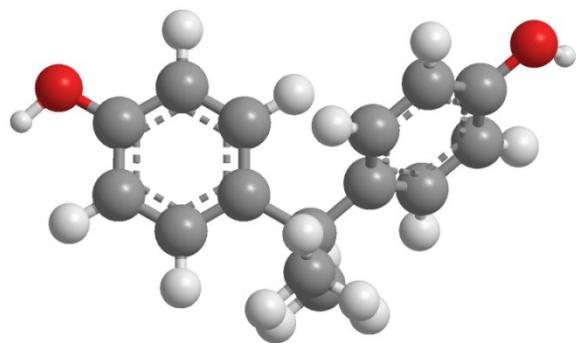
Fig. S1 Molecular structure of BPA.
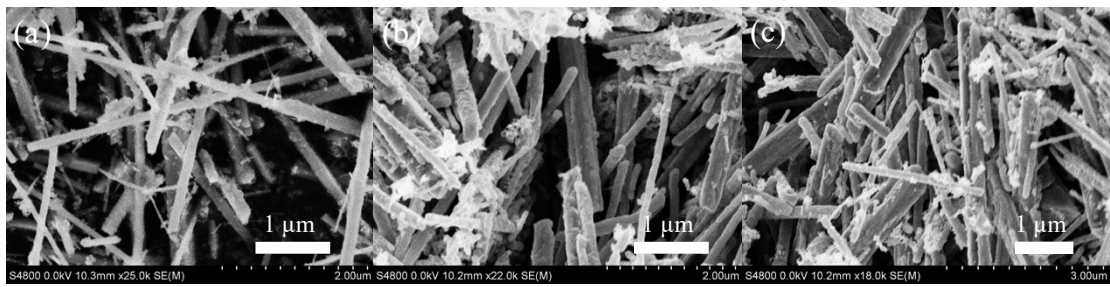
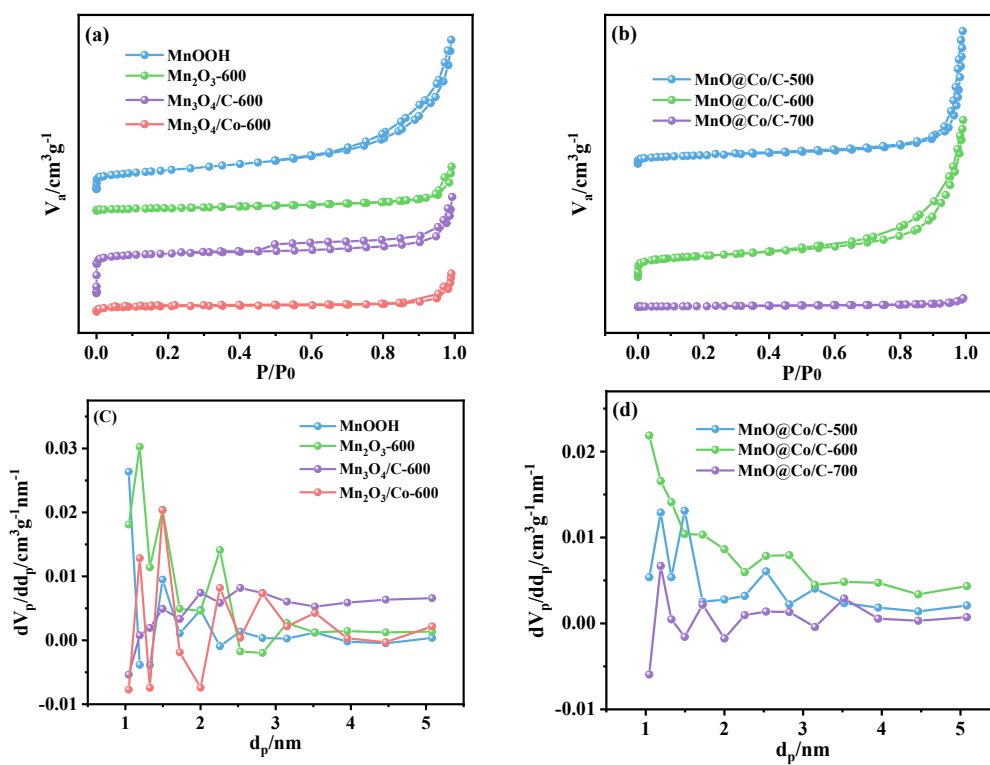**Fig S2**. SEM images of (a) MnOOH, (b) Mn_2O_3-600, (c) Mn_3O_4/Co-600.

Fig. S3 (a, b) N_2 adsorption/desorption isotherm and (c, d) corresponding pore size distribution curves of comparative catalysts: MnOOH, Mn_2O_3-600, Mn_3O_4/C-600, Mn_2O_3/Co-600, MnO@Co/C-500, MnO@Co/C-600, and MnO@Co/C-700.
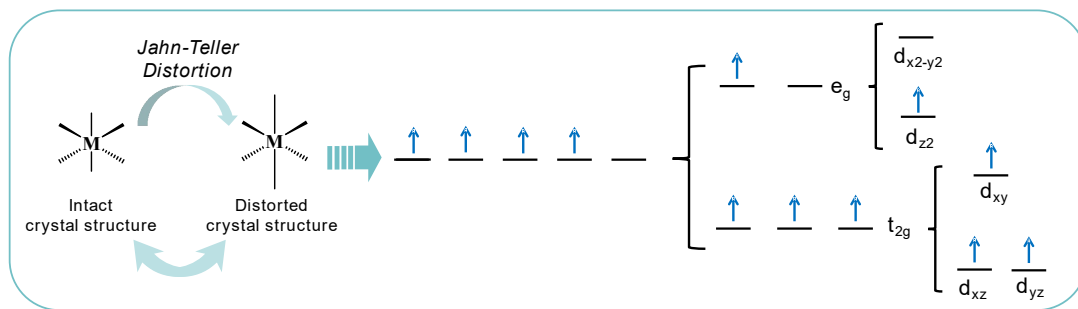
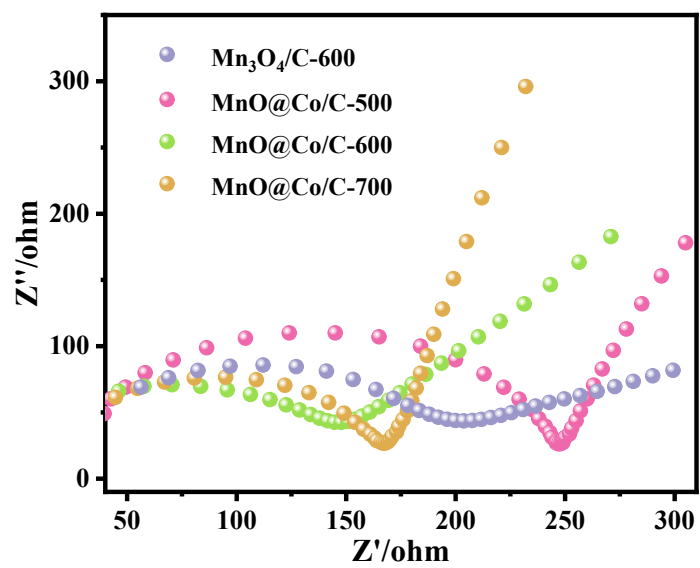**Fig. S4** Jahn-Teller distortions for octahedral Mn complex.

Fig. S5 Electrochemical impedance spectra (EIS) for different samples.
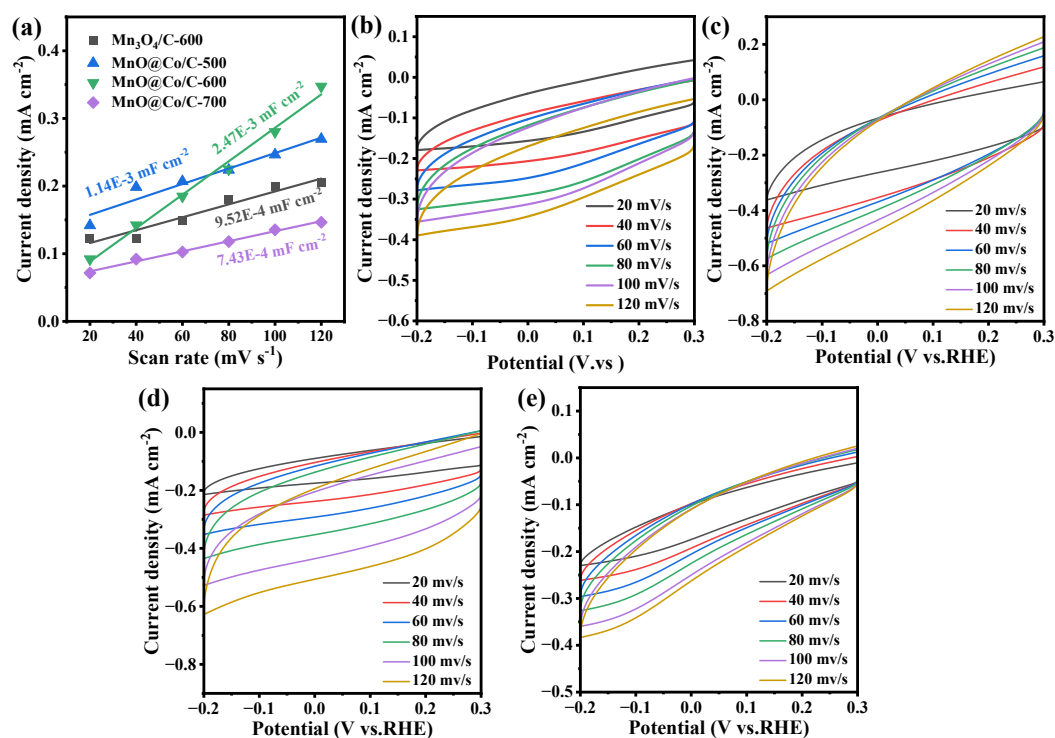
Fig. S6 Charging current density difference and cyclic voltammetry (CV) scanning rate of catalysts: (a) analysis of the electrochemical active surface area (ECSA): Cyclic voltammetric curves for different scan rates (20-120 mV s^{-1}) and (b) Mn$_3$O$_4$/C-600, (c) MnO@Co/C-500, (d)MnO@Co/C-600, (e) MnO@Co/C-700 samples in the range from -0.2 to 0.3 V vs. RHE.
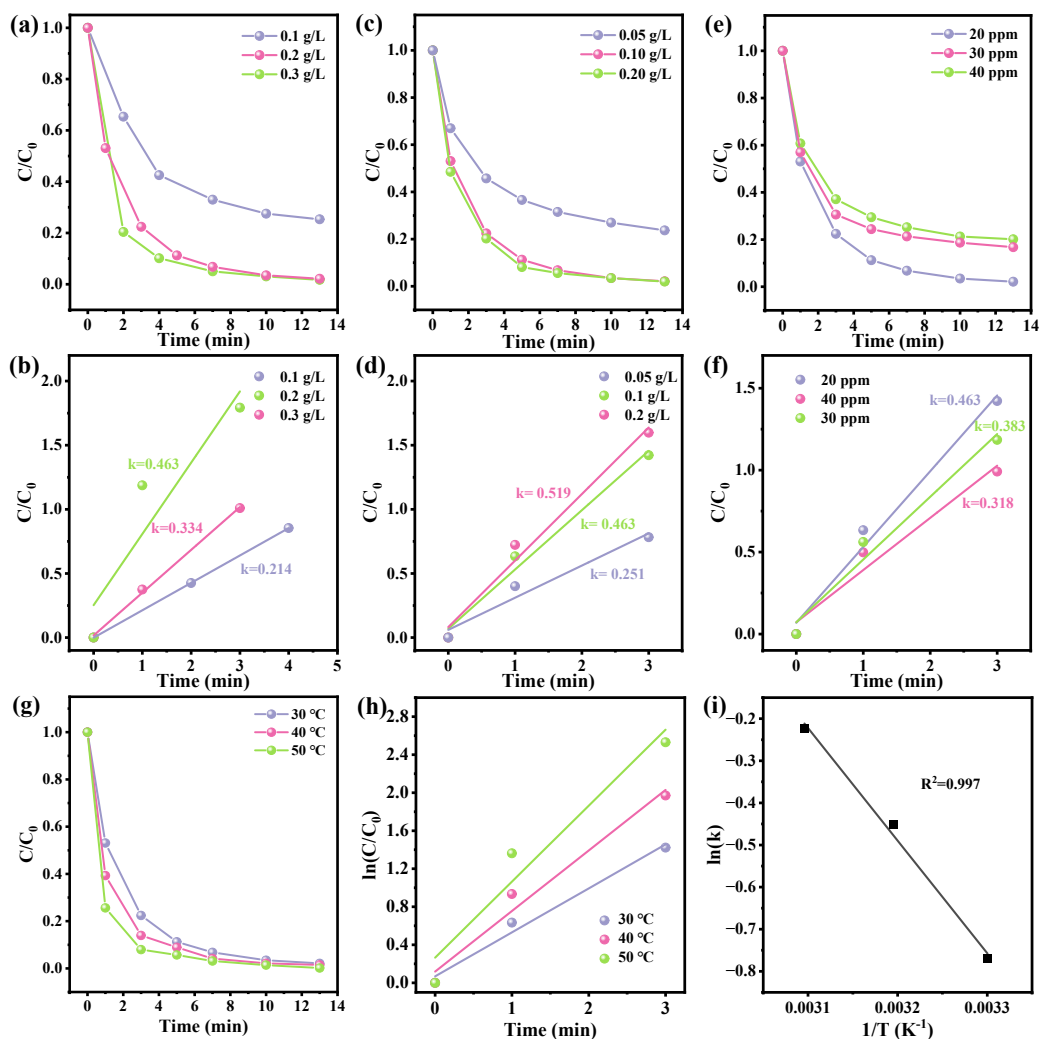
Fig. S7 (a) Time-dependent BPA degradation course curves over MnO@Co/C-600 using different PMS dosages, and (b) the corresponding kinetic curves: $\ln(C_0/C)$ v.s. reaction time; reaction condition: [BPA] = 20 mg L^{-1}, [catalyst] = 0.1 g L^{-1}. (c) Time-dependent BPA degradation course curves over MnO@Co/C-600 using catalyst dosages, and (d) the corresponding kinetic curves: $\ln(C_0/C)$ v.s. reaction time; reaction condition: [BPA] = 20 mg L^{-1}, [PMS] = 0.2 g L^{-1}. (e) Time-dependent BPA degradation course curves over MnO@Co/C-600 using different BPA concentration, and (f) the corresponding kinetic curve: $\ln(C_0/C)$ v.s. reaction time; reaction condition: [catalyst] = 0.1 g L^{-1}, [PMS] = 0.2 g L^{-1}. (g) Time-dependent BPA degradation course curves over MnO@Co/C-600 using different BPA concentration, and (h) the corresponding kinetic curve: $\ln(C_0/C)$ v.s. reaction time; reaction condition: [catalyst] = 0.1 g L^{-1}, [PMS] = 0.2 g L^{-1}. (i) Arrhenius plots derived from corresponding kinetic curves of MnO@Co/C-6000: $\ln(k)$ v.s. T^{-1}
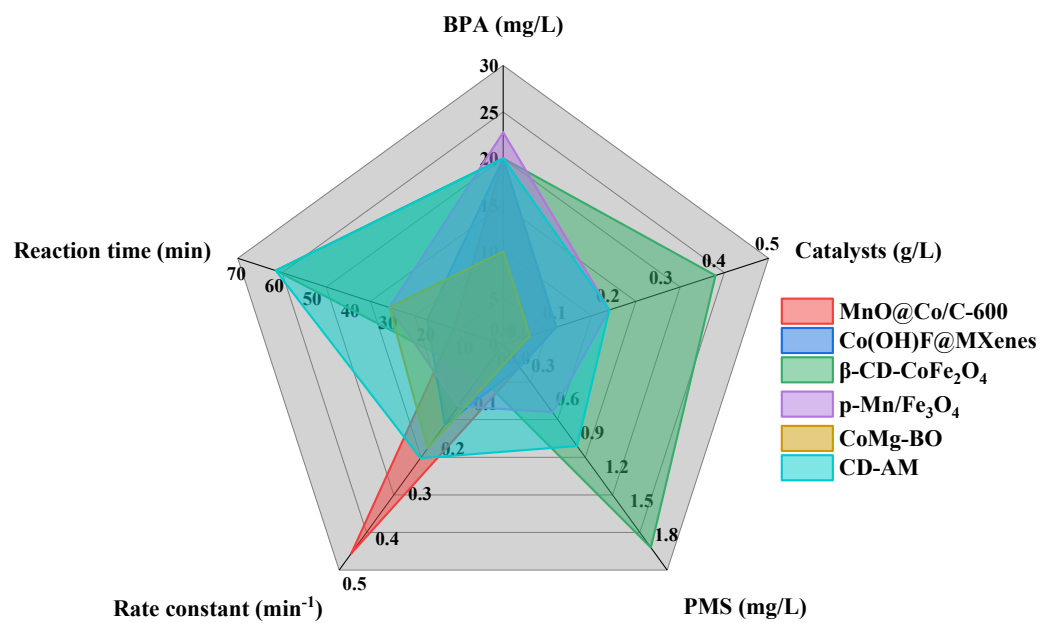
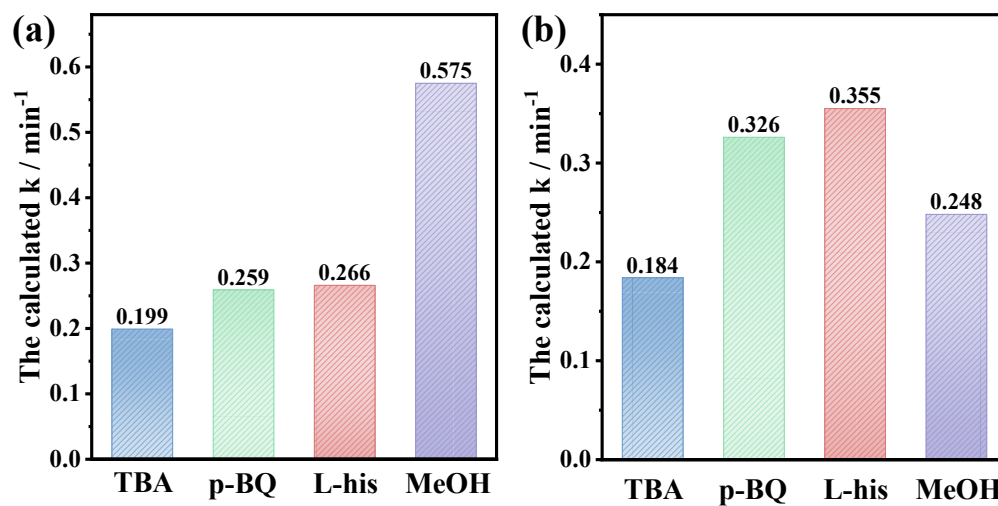**Fig. S8** Comparison of different catalysts activating PMS to remove BPA.

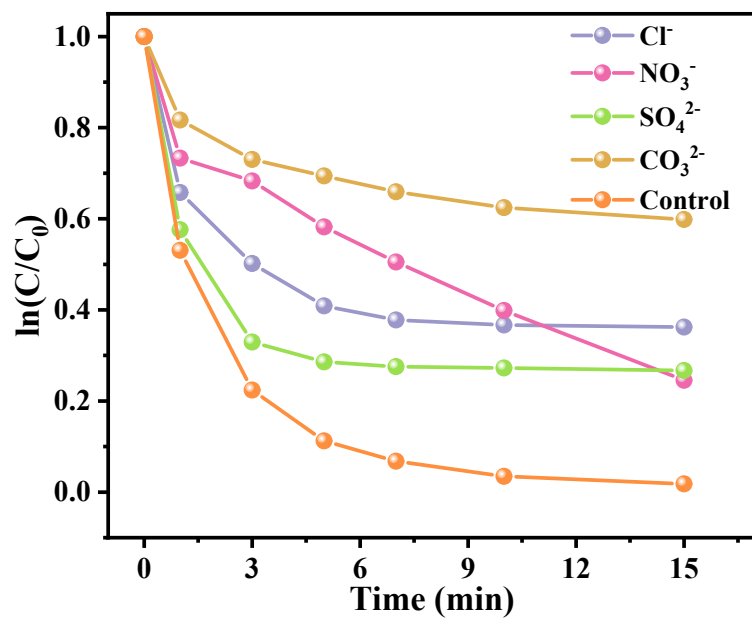**Fig. S9** Contribution of different quenchers to quenched active radicals.

Fig. S10 Time-dependent BPA degradation course curves over MnO@Co/C-600 using different anion.
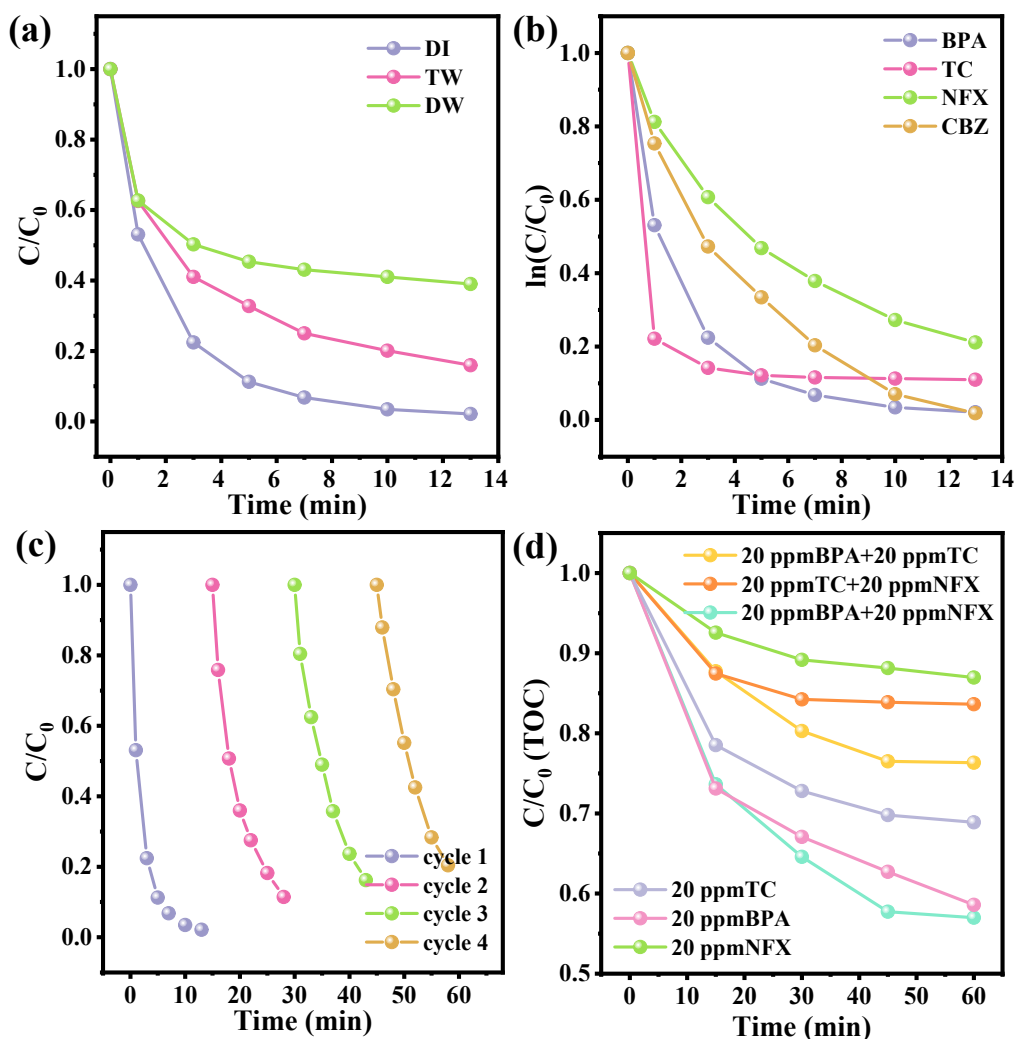
Fig. S11 (a) Degradation progress curves of BPA using the MnO@Co/C-600 system in authentic water samples; reaction conditions: [BPA] = 20 mg L^{-1}, [PMS] = 0.2 g L^{-1}, [catalyst] = 0.1 g L^{-1}, Temperature = 25 °C. (b) Degradation progress curves of different pollutants in the MnO@Co/C-600 system; reaction conditions: [pollutants] = 20 mg L^{-1}, [PMS] = 0.2 g L^{-1}, temperature = 25 °C. (c) Results of cycling experiments with MnO@Co/C-600 in activating PMS for BPA degradation; reaction conditions: [BPA] = 20 mg L^{-1}, [PMS] = 0.2 g L^{-1}, [catalyst] = 0.1 g L^{-1}, temperature = 25 °C. (d) Total Organic Carbon (TOC) removal progress curves using the MnO@Co/C-600 system for different pollutants; Reaction conditions: [PMS] = 0.2 g L^{-1}, [catalyst] = 0.1 g L^{-1}, temperature = 25 °C.
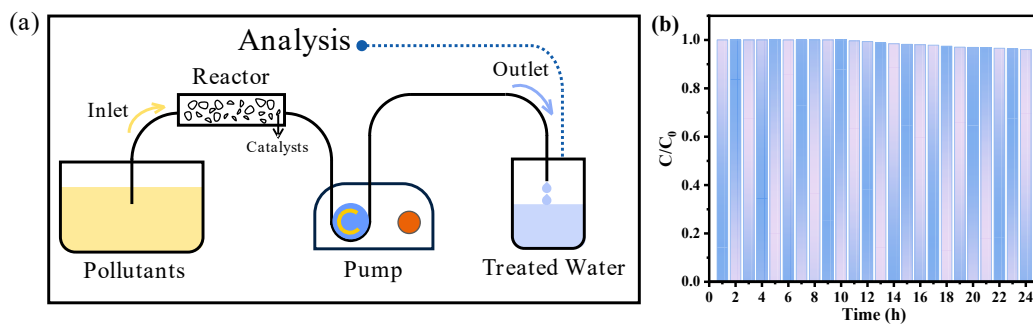
Fig. S12 (a) The schematic diagram of circulation filter integrated device; (b) BPA degradation course curves by MnO@Co/C-600 system under flow-through conditions; Reaction condition: [BPA] = 5 mg L^{-1}, [PMS] = 0.2 g L^{-1}, [catalyst] = 20 mg, Temperature = 25 °C.
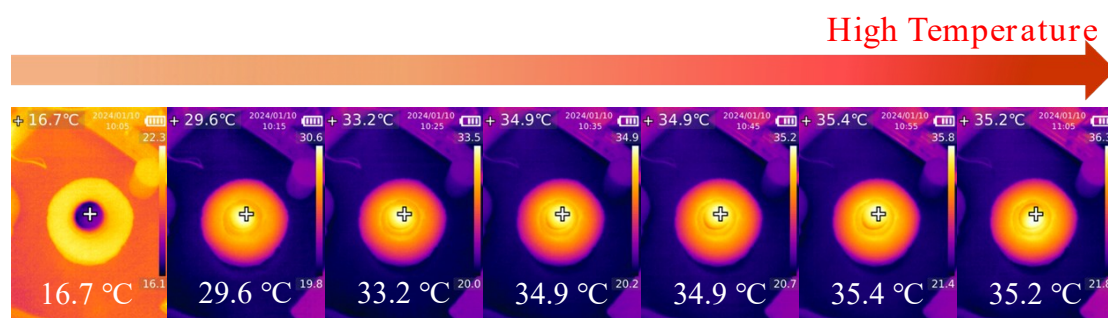
Fig. S13 Time-dependent surface temperature thermal IR images of wet MnO@Co/C-600 samples under one sun irradiation in air.